The Effects of Transverse Shear on the Delamination of Edge-Notch Flexure and 3-Point Bend Geometries

M. D. Thouless
Department of Mechanical Engineering
Department of Materials Science & Engineering
University of Michigan
Ann Arbor, MI 48109

January 29, 2009

Abstract

A general approach to develop complete and rigorous analytical expressions for the energy-release rates and phase angles for delamination of isotropic beam-like geometries is summarized. The analysis allows the effects of transverse shear to be correctly incorporated within the resulting expressions. The approach requires four effective crack-tip loads to be determined from the applied loads: a moment, an axial force, a double transverse shear force, and a single transverse shear force. Each of these effective loads provides an energy-release rate and an associated phase angle; expressions for these quantities can be found in the literature. These fundamental expressions can be combined algebraically to generate analytical expressions for the total energy-release rate and phase angle for any geometry and loading configuration of interest. The approach is illustrated by general analyses of edge-notched flexure (ENF), end-loaded split (ELS) and 3-point bending specimens. In particular, it is shown that the equation for the energy-release rate for the ENF geometry reduces to a very simple form that has previously been proposed from numerical studies, when the geometry is perfectly anti-symmetrical.

Keywords: [A] Layered structures; [B] Fracture; [B] Delamination; Shear

1 Introduction

1.1 Analyses of the edge-notch flexure geometry

The general geometry of an edge-notch flexure (ENF) specimen is shown in Fig. 1(a). Two laminates, with thicknesses h_1 and h_2 are bonded together with a debond of length a extending from one end. The moduli of the two arms are $\bar{E}_1$ and $\bar{E}_2$, respectively, where $\bar{E}$ is the plane-stress or plane-strain modulus, as appropriate. The beam is simply supported at both ends, with a point load, F (per unit width), applied to its mid-point.[1] The special case of an anti-symmetrical geometry, with $h_1 = h_2 = h$ and $\bar{E}_1 = \bar{E}_2 = \bar{E}$, is frequently used to evaluate the mode-II toughness of an interface. Under these conditions, each arm is subjected to a transverse shear force of $F/4$ and a moment of $Fa/4$ immediately behind the crack tip, while the section immediately ahead of the crack tip is subjected to a transverse shear force of $F/2$ and a moment of $Fa/2$. If the crack is very long compared to the height of the two arms, the shear component at the crack tip can be neglected. A steady-state energy balance can then be used to show that the energy-release rate is given by

$$\mathcal{G} = \frac{9}{16}\frac{F^2a^2}{\bar{E}h^3}. \tag{1}$$

Furthermore, the perfect asymmetry of the problem confirms that the phase angle associated with this loading is 90°, or pure mode-II.

It has long been recognized that the transverse shear load provides a correction to this result. Carlsson *et al.* [1] developed an analysis based on Timoshenko beam theory to derive an expression for the energy-release rate that incorporates a term associated with shear:

$$\mathcal{G} = \frac{9}{16}\frac{F^2a^2}{\bar{E}h^3}\left[1 + 0.2(E/G)(h/a)^2\right], \tag{2}$$

where G is the interlaminar shear modulus. As expected, this expression reduces to Eqn. 1 when the crack is long enough for the moment contribution to dominate the shear contribution. An alternative approach that has been proposed for analyzing this geometry involves modeling half the specimen as a beam lying on an elastic foundation, and then including the deformation of this foundation in the calculation of the energy-release rate. As pointed out by Li *et al.* [2] only the shear contribution of the energy-release rate is affected by the properties of the foundation in such a model, so this approach has the feature of providing what is essentially a shear correction to Eqn. 1. However, while the elastic-foundation approach provides a simple expression

[1] The analysis given in this paper assumes symmetry about the mid-point of the beam. Strictly speaking, the ENF geometry with a single split doesn't satisfy this symmetry condition, although a clamped split beam would satisfy it. This issue is ignored for the small elastic deformations assumed in this paper.

for the energy-release rate of the mode-I double-cantilever beam geometry [3, 4], it does not appear to provide a simple form for the energy-release rate of the mode-II ENF geometry [5, 6]. Furthermore, there is no *a priori* method to determine the value of the parameters to describe the appropriate stiffness of the foundation. They have to be obtained by a comparison to numerical analyses of the geometry.

Comparisons to numerical analyses of the ENF geometry indicate that the following expression for the energy-release rate is very accurate [7]:

$$\mathcal{G} = \frac{9}{16}\frac{F^2 a^2}{\bar{E}h^3}\left[1 + 0.209h/a\right]^2 . \tag{3}$$

Andrews and Massabò [8] have already shown that this equation can be derived by incorporating the effects of shear into the calculation for the energy-release rate. The shear correction has two components: (i) a steady-state energy term and (ii) a term arising from the interaction of the shear force with the root rotation at the crack tip. The first term is independent of crack length (as captured in the form of Eqn. 2); the second term scales with the crack length. The bending moment at the crack tip associated with the applied transverse shear force provides a term in the energy-release rate that scales with the square of the crack length (as indicated in the form of Eqn. 1). Only in special geometries does the functional form of the combined contributions reduce to the perfect square of Eqn. 3. The symmetrical double-cantilever beam is another example of a geometry where the shear correction reduces in a similar fashion [2].[2]

A general analysis for the energy-release rate and phase angle associated with transverse shear on isotropic beam-like geometries was developed by Li *et al.* [2]. It was demonstrated that, by combining these results with the earlier results of Suo and Hutchinson [10] for the energy-release rate and phase angle associated with axial loads and moments, analytical results for the phase angle and energy-release rate of arbitrarily-loaded beam-like geometries could be determined. However, the examples given in Ref. [2] were fairly straight-forward applications of the analytical technique, with a focus on symmetrical and asymmetrical double-cantilever beam geometries. The geometries presented in this paper complement these solutions and are much richer in terms of the analysis. The primary purpose of this paper is to demonstrate how to combine the results of Suo and Hutchinson [10] with those of Li *et al.* [2] when analyzing general beam-like geometries. This is done by first calculating analytical expressions for the energy-release rate and phase angle of edge-notched flexure geometries. A second set of calculations is done for the delamination of an end-loaded split

[2]The reduction to such a simple form results in the notion that one can use Eqn. 1 with a correction to the crack length providing the extra compliance required to model the additional contribution to the energy-release rate from the transverse-shear loading [9]. This simple description of the effects of shear as a change in the effective crack length is an artifact of the special case in which the equation for the energy-release rate simplifies in a particularly elegant fashion.

(ELS) specimen. The final set of calculations is done for delamination of three-point bend specimens.

1.2 Effect of shear on delamination of beam-like geometries

Any arbitrary loading on a beam-like geometry consisting of two bonded layers can be expressed as a set of moments, M_1, M_2, M_3, axial forces, N_1, N_2, N_3 and shear forces, V_1, V_2, V_3, acting on the laminates immediately behind and ahead of a delamination front (Fig. 2). If the layers are isotropic and linear elastic, these nine loads can further be reduced to a set of four effective loads: an axial load (Fig. 3a), N, a bending moment (Fig. 3b), M, a double transverse shear load (Fig. 3c), V_d, and a single transverse shear load (Fig. 3d), V_s. If the two layers are of thickness h_1 and h_2, with elastic constants of E_1, ν_1, E_2 and ν_2, the effective loads are related to the original set of loads by

$$\begin{aligned} M &= M_1 - C_3 M_3 \\ N &= N_1 - C_1 N_3 - C_2 M_3/h_1 \\ V_d &= V_1 - V_3 \\ V_s &= V_3 \end{aligned} \tag{4}$$

where [10],

$$\begin{aligned} C_1 &= \frac{\Sigma H}{1+\Sigma H} \\ C_2 &= \frac{\Sigma H^2}{\tilde{I}_{(2)}}\left[1-\Delta+\frac{H}{2}\right] \\ C_3 &= \frac{\Sigma H^3}{12\tilde{I}_{(2)}} \end{aligned} \tag{5}$$

and,

$$\begin{aligned} \Sigma &= \bar{E}_1/\bar{E}_2 \\ H &= h_1/h_2 \\ \Delta &= \frac{1+2\Sigma H+\Sigma H^2}{2(1+\Sigma H)} \\ \tilde{I}_{(2)} &= \frac{1}{3}\left\{\Sigma\left[(H+1-\Delta)^3-(1-\Delta)^3\right]+\Delta^3+(1-\Delta)^3\right\}. \end{aligned} \tag{6}$$

The energy-release rate and phase angle resulting from these four effective crack-tip loads can be found by a superposition of the four corresponding standard solutions

that exist in the literature. The results of Suo and Hutchinson [10] can be used to determine the energy-release rate for the steady- state problems associated with the bending moment and axial load:

$$\begin{aligned} \mathcal{G}_M &= f_M^2(\alpha, H)\frac{M^2}{\bar{E}_1 {h_1}^3} \\ \mathcal{G}_N &= f_N^2(\alpha, H)\frac{N^2}{\bar{E}_1 h_1} \\ \psi_M &= \psi_M(\alpha, \beta, H) \\ \psi_N &= \psi_P(\alpha, \beta, H), \end{aligned} \tag{7}$$

where α is the first Dundurs parameter [11], given by $\alpha = (\Sigma - 1)/(\Sigma + 1)$, and β is the second Dundurs parameter [11]. The non-dimensional functions, $f_M(\alpha, H)$ and $f_N(\alpha, H)$, can be found from a steady-state energy balance [10] as

$$\begin{aligned} f_M(\alpha, H) &= \sqrt{6(1 + \Sigma H^3)} \\ f_N(\alpha, H) &= \sqrt{0.5 + \Sigma(1.5H^3 + 3H^2 + 2H)}. \end{aligned} \tag{8}$$

A steady-state energy balance can also be used to show that the two phase angles are related by

$$\cos\zeta_{NM} = \cos(\psi_N - \psi_M) = \frac{3\Sigma H^2(1 + H)}{f_N f_M}, \tag{9}$$

leaving only one phase angle to be determined numerically [10]. It should be noted that the absence of the second Dundurs parameter, β, from an expression indicates that it can be derived from a steady-state energy balance, and that the expression does not depend on the details of the crack-tip stress field or deformation.

The second two standard solutions are those associated with the double transverse shear load (Fig. 3c) and the single transverse shear load (Fig. 3d). The energy-release rate and phase angle associated with the double transverse shear load are [2]

$$\begin{aligned} \mathcal{G}_{V_d} &= {f_{V_d}}^2(\alpha, \beta, H)\frac{{V_d}^2}{\bar{E}_1 h_1} \\ \psi_{V_d} &= \psi_{V_d}(\alpha, \beta, H). \end{aligned} \tag{10}$$

The corresponding results for the single transverse shear load are [2]

$$\begin{aligned} \mathcal{G}_{V_s} &= {f_{V_s}}^2(\alpha, \beta, H)\frac{{V_s}^2}{\bar{E}_1 h_1} \\ \psi_{V_s} &= \psi_{V_s}(\alpha, \beta, H). \end{aligned} \tag{11}$$

The dimensionless functions for the energy-release rates and the phase angles must be calculated numerically, since there are no steady-state energy-balance solutions

for transverse shear loading, and the solutions depend on the details of the crack-tip deformations. This is indicated by the dependence of the solutions on β. The values of $f_{V_d}(\alpha,0,H)$, $f_{V_s}(\alpha,0,H)$, $\psi_{V_d}(\alpha,0,H)$ and $\psi_{V_s}(\alpha,0,H)$ are given in Ref. [2]. They are reproduced for convenience in the Appendix of this paper, along with $\psi_M(\alpha,0,H)$.

The total energy-release rate, $\mathcal{G}$, and the net phase angle, ψ, of a beam-like geometry subjected to any combination of the four loading conditions can be found by adding the individual components in a vectorial fashion. The energy-release rate and phase angle are given by

$$\mathcal{G} = \mathcal{G}_1 + \mathcal{G}_2 \tag{12}$$

$$\psi = \tan^{-1}\left(\sqrt{\mathcal{G}_2}/\sqrt{\mathcal{G}_1}\right) \tag{13}$$

where,

$$\begin{aligned}
\sqrt{\mathcal{G}_1} &= \sqrt{\mathcal{G}_M}\cos(\psi_M) + \sqrt{\mathcal{G}_N}\cos(\psi_N) + \sqrt{\mathcal{G}_{V_d}}\cos(\psi_{V_d}) + \sqrt{\mathcal{G}_{V_s}}\cos(\psi_{V_s}) \\
\sqrt{\mathcal{G}_2} &= \sqrt{\mathcal{G}_M}\sin(\psi_M) + \sqrt{\mathcal{G}_N}\sin(\psi_N) + \sqrt{\mathcal{G}_{V_d}}\sin(\psi_{V_d}) + \sqrt{\mathcal{G}_{V_s}}\sin(\psi_{V_s})
\end{aligned} \tag{14}$$

The sign of the phase angles given in the literature and Appendix (with $-90^\circ < \psi_N < 90^\circ$) are for positive values of M, N, V_d and V_s as defined in Fig. 3. Individual phase angles must be rotated by 180° if any of the corresponding loading parameters are in the opposite sense from those shown in Fig. 3.

These expressions are valid for any isotropic linear-elastic geometry, provided the loads and moments at the crack tip can be correctly calculated. The results appear to be correct even when the length of the debond is comparable to the layer thickness, provided steady-state stress distributions have been achieved in the layers [2]. In particular, it should be noted that all root rotation effects are implicitly included in the expressions for the energy-release rates and phase angles. While root rotation is induced by all four types of loading, it only affects the energy-release rate associated with transverse shear. This is directly related to the observation that the energy-release rate for the axial load and the moment can be derived from a steady-state energy balance, but the energy-release rate for the shear terms depends on the stress field at the crack-tip. The interaction between the shear loads and the root rotation associated with the other loads is incorporated by the phase angles. Andrews and Massabò [8] have developed an equivalent approach for including the effects of shear in which this interaction is made explicit.

2 Analysis of ENF geometry

The loads and moments acting at the crack tip of the ENF specimen shown in Fig. 1(a) are given by $M_1 = F_1 a$, $M_2 = F_2 a$, $M_3 = Fa/2$, $V_1 = F_1$, $V_2 = F_2$ and $V_3 = F/2$,

where F_1 and F_2 are found by matching the displacements of the two arms at the crack mouth where the specimen is supported:

$$\begin{aligned} F_1 &= \frac{AF}{2} = \frac{\Sigma H^3}{1+\Sigma H^3}\frac{F}{2} \\ F_2 &= \frac{(1-A)F}{2} = \frac{1}{1+\Sigma H^3}\frac{F}{2} \end{aligned} \tag{15}$$

This results in an effective crack-tip loading of

$$\begin{aligned} M &= (A-C_3)\frac{Fa}{2} \\ N &= -\frac{C_2}{h_1}\,\frac{Fa}{2} \\ V_d &= -(1-A)F/2 \\ V_s &= F/2 \end{aligned} \tag{16}$$

The sign convention on these equations is established by Fig. 3, which illustrates the positive directions for all loads and moments.

Equations 7 through 11 can then be used to express the individual components of the energy-release rate in terms of the geometry and loads applied to the ENF geometry of Fig. 1a:

$$\begin{aligned} \frac{\bar{E}_1 {h_1}^3 \mathcal{G}_M}{F^2 a^2} &= \frac{(A-C_3)^2}{4} {f_M}^2 \\ \frac{\bar{E}_1 {h_1}^3 \mathcal{G}_N}{F^2 a^2} &= \frac{C_2^2}{4} {f_N}^2 \\ \frac{\bar{E}_1 {h_1}^3 \mathcal{G}_{V_d}}{F^2 a^2} &= \frac{(1-A)^2 (h_1/a)^2}{4} f_{V_d}^2 \\ \frac{\bar{E}_1 {h_1}^3 \mathcal{G}_{V_s}}{F^2 a^2} &= \frac{(h_1/a)^2}{4} f_{V_s}^2 \end{aligned} \tag{17}$$

Eqn. 14 then gives the two orthogonal modes of the energy-release rate:

$$\begin{aligned} \sqrt{\frac{\bar{E}_1 {h_1}^3 \mathcal{G}_1}{F^2 a^2}} = \quad & 0.5[(A-C_3) f_M \cos(\psi_M) - C_2 f_N \cos(\psi_N) \\ & -(1-A)(h_1/a) f_{V_d} \cos(\psi_{V_d}) + (h_1/a) f_{V_s} \cos(\psi_{V_s})] \\ \sqrt{\frac{\bar{E}_1 {h_1}^3 \mathcal{G}_2}{F^2 a^2}} = \quad & 0.5[(A-C_3) f_M \sin(\psi_M) - C_2 f_N \sin(\psi_N) \\ & -(1-A)(h_1/a) f_{V_d} \sin(\psi_{V_d}) + (h_1/a) f_{V_s} \sin(\psi_{V_s})] \end{aligned} \tag{18}$$

Eqns. 12 through 14 can then be used to calculate the total energy-release rate and phase angle.

The resulting expression for the energy-release rate can be simplified for the limiting case of a very long crack, when the shear contribution is negligible. It is given by

$$\frac{\bar{E}_1 {h_1}^3 \mathcal{G}}{F^2 a^2} = \frac{\Sigma H^3}{2}\left[\frac{3}{1+\Sigma H^3} - \frac{1}{4\tilde{I}_{2)}}\right] \tag{19}$$

More general results including the effects of shear are plotted for some special cases in Figs. 4 and 5. In all cases the asymptotic limits at large values of a/h_1 correspond to Eqn. 19. It can be seen from these figures that the effects of shear are important for crack lengths less than about $10h_1$.

A simplified equation for the special case of a homogeneous geometry with arms of equal thickness can be obtained by setting $\bar{E}_1 = \bar{E}_2 = \bar{E}$ and $h_1 = h_2 = h$. The parameters then have the following values:

$$\begin{aligned}
A &= 0.5 \\
C_2 &= 3/4 \\
C_3 &= 1/8 \\
f_M &= \sqrt{12} = 3.464 \\
f_N &= \sqrt{7} = 2.646; \\
f_{V_d} &= 2.335; \\
f_{V_s} &= 1.207; \\
\psi_M &= 0.0^\circ \\
\psi_N &= 49.107^\circ \\
\psi_{V_d} &= 0.0^\circ \\
\psi_{V_s} &= -15.1^\circ.
\end{aligned} \tag{20}$$

So that the components $\mathcal{G}_1$ and $\mathcal{G}_2$ are

$$\begin{aligned}
\sqrt{\frac{\bar{E}_1 h^3 \mathcal{G}_1}{F^2 a^2}} &= 0.00 \\
\sqrt{\frac{\bar{E}_1 h^3 \mathcal{G}}{F^2 a^2}} &= 0.5[-1.500 - 0.314h/a],
\end{aligned} \tag{21}$$

and the energy-release rate is

$$\frac{\bar{E}_1 {h_1}^3 \mathcal{G}}{F^2 a^2} = \frac{9}{16}[1 + 0.210h/a]^2. \tag{22}$$

This is identical (with the shear term agreeing to within a fraction of a percent) to Eqn. 3. This particular form of the equation, that makes the shear term look like a simple correction to the crack length, is the result of one mode of the energy-release

rate being equal to zero. As discussed above, the functional relationship between the energy-release rate and crack length can't generally be expressed as a perfect square, and the apparent connection between the shear contribution and a change in effective crack length is lost.

It should be noted that the correction term associated with shear occurs in the absence of any interfacial compliance, and that only this correction term can be affected by interfacial compliance. This point is important in any discussion about mechanics models that include the effects of different types of interfacial bonding, the compliance of an adhesive layer, or the rotation at the crack tip. In particular, analyses that attempt to capture the effect of a compliant adhesive layer [12] or cohesive zone, must be cast in the form of corrections to the shear term only [2, 13]. In the limit of rigid interfaces, these analyses must reduce to a form that contains a shear correction. Several models in the literature do not apparently reduce to such a form; the absence of a shear term then raises the question of whether the models might have an internal inconsistency since it is only the shear term that can be affected by interfacial compliance. This is a general observation that is valid for assessing interface models for all types of beam-like geometries, whether they are mode-I, mode-II or mixed-mode geometries.

3 Analysis of end-loaded split specimen

The general geometry of an end-loaded split (ELS) specimen is shown in Fig. 1b. A beam, consisting of two laminates (with thicknesses h_1 and h_2 and moduli $\bar{E}_1$ and $\bar{E}_2$) bonded together, is clamped at one end and contains a delamination of length a at the other end. A load F is applied to only one arm to cause delamination. Since the general results in the Appendix are limited to cases for which $H < 1$, two types of effective loads have to be considered, depending on whether h_1 is greater or less than h_2. If $h_1 < h_2$, the crack-tip loading is $M_1 = M_3 = Fa$, and $V_1 = V_3 = F$; the results of the Appendix can then be used directly with

$$\begin{aligned} M &= (1 - C_3)Fa \\ N &= -C_2 Fa/h_1 \\ V_d &= 0 \\ V_s &= F. \end{aligned} \tag{23}$$

If $h_1 > h_2$, the crack-tip loading is $M_2 = Fa$, $M_3 = -Fa$, $V_2 = F$, and $V_3 = -F$; the results of the Appendix can then be used with

$$\begin{aligned} M &= C_3 Fa \\ N &= C_2 Fa/h_1 \end{aligned}$$

$$\begin{aligned} V_d &= F \\ V_s &= -F, \end{aligned} \tag{24}$$

and a recognition that this represents a specimen that has been flipped upside down (changing the sign of the phase angle).

For a homogenous specimen with $h_1 = h_2 = h$ and $\bar{E}_1 = \bar{E}_2 = \bar{E}$, the energy-release rate and phase angle can be shown to be given by

$$\begin{aligned} \frac{\bar{E}\mathcal{G}h^3}{F^2a^2} &= 5.250 + 4.989(h/a) + 1.462(h/a)^2 \\ \psi &= \tan^{-1}\left(\frac{-\sqrt{3}(1+0.210h/a)}{2(1+0.674h/a)}\right) \end{aligned} \tag{25}$$

This is essentially identical to the result quoted in Ref. [7], and can be derived by recognizing that the solution for the ELS geometry can be obtained from a superposition of the pure mode-I double-cantilever beam configuration [2] and the pure mode-II ENF configuration. This geometry provides an example of the general relationship between energy-release rate and crack length, where the shear correction cannot be expressed in terms of a simple change in the effective crack length. Figures 6 and 7 show plots for the energy-release rate and phase angle for more general configurations of this specimen.

4 Analysis of 3-point bend geometry

The geometry of a 3-point bend specimen is shown in Fig. 1(c). A beam of length $2L$, consisting of two laminates (with thicknesses h_1 and h_2 and moduli $\bar{E}_1$ and $\bar{E}_2$) bonded together, is simply supported at both ends and supports a point load, F, in the center. One laminate is completely cracked up to the interface, and a debond of length a extends symmetrically along the interface from this crack. As mentioned in the previous section, the results in the Appendix are limited to $h_1/h_2 < 1$ so two geometries need to be analyzed: one in which the thicker laminate is fractured so that $M_1 = M_3 = F(L-a)/2$, and $V_1 = V_3 = -F/2$, the other in which the thinner laminate is fractured so that $M_2 = F(L-a)/2$, $M_3 = -F(L-a)/2$, and $V_2 = V_3 = F/2$.

Following the procedures of the previous sections, the loads and moments in the fundamental solutions for the first of these geometries can be expressed as:

$$\begin{aligned} M &= (1-C_3)\frac{F(L-a)}{2} \\ N &= -\frac{C_2}{h_1}\,\frac{F(L-a)}{2} \end{aligned}$$

$$\begin{aligned} V_d &= 0 \\ V_s &= -F/2, \end{aligned} \tag{26}$$

with C_2 and C_3 defined in Eqn. 5. As before, Eqns. 7 through 11 can be used to express the energy-release rate and phase angle in terms of the individual components of the energy-release rate:

$$\begin{aligned} \frac{\bar{E}_1 {h_1}^3 \mathcal{G}_M}{F^2 L^2} &= \frac{(1-C_3)^2}{4}(1-a/L)^2 {f_M}^2 \\ \frac{\bar{E}_1 {h_1}^3 \mathcal{G}_N}{F^2 L^2} &= \frac{C_2^2}{4}(1-a/L)^2 {f_N}^2 \\ \frac{\bar{E}_1 {h_1}^3 \mathcal{G}_{V_d}}{F^2 L^2} &= 0 \\ \frac{\bar{E}_1 {h_1}^3 \mathcal{G}_{V_s}}{F^2 L^2} &= \frac{(h_1/L)^2}{4} f_{V_s}^2. \end{aligned} \tag{27}$$

For geometries in which the cracked laminate is thinner than the uncracked laminate, it can be shown that the appropriate equations are

$$\begin{aligned} M &= C_3 \frac{F(L-a)}{2} \\ N &= \frac{C_2}{h_1} \frac{F(L-a)}{2} \\ V_d &= -F/2 \\ V_s &= F/2. \end{aligned} \tag{28}$$

So that,

$$\begin{aligned} \frac{\bar{E}_1 {h_1}^3 \mathcal{G}_M}{F^2 L^2} &= \frac{C_3^2}{4}(1-a/L)^2 {f_M}^2 \\ \frac{\bar{E}_1 {h_1}^3 \mathcal{G}_N}{F^2 L^2} &= \frac{C_2^2}{4}(1-a/L)^2 {f_N}^2 \\ \frac{\bar{E}_1 {h_1}^3 \mathcal{G}_{V_d}}{F^2 L^2} &= \frac{(h_1/L)^2}{4} f_{V_d}^2 \\ \frac{\bar{E}_1 {h_1}^3 \mathcal{G}_{V_s}}{F^2 L^2} &= \frac{(h_1/L)^2}{4} f_{V_s}^2. \end{aligned} \tag{29}$$

As in the previous sections, the quadrants of the individual phase angles are established by the signs of the appropriate loads in Eqns. 26 and 28. This second configuration represents a specimen that has been flipped up-side down, changing the sign of the resultant phase angle.

Three non-dimensional length parameters affect the mechanics of the three-point bend geometry. In addition to the thickness ratio, $H = h_1/h_2$, and crack length, a/L, the span length, L/h_1, also plays an important role in the fracture mechanics of this geometry. The effects of transverse shear can be neglected in the limits that the span is very long, $L/h_1 \to \infty$, and the crack is relatively short, $a/L << 1$. Under these conditions, the energy-release rate is given by

$$\frac{\bar{E}_1 {h_1}^3 \mathcal{G}}{F^2 L^2} = \left(1 - \frac{a}{L}\right)^2 \left(\frac{3}{2} - \frac{\Sigma H^3}{8\tilde{I}_{(2)}}\right) \tag{30}$$

The three-point bending geometry is one that exhibits stable crack growth; the energy-release rate decreases as the crack extends. Figure 8 shows how the energy-release rate and phase angle vary as functions of the non-dimensional span length, at the point at which the crack extends half way across the span. The limiting steady-state solutions corresponding to Eqn. 30 have been added to these plots in the form of dotted lines at large values of the span length. One of the points that will be noticed from this figure is that the effect of transverse shear is to *reduce* the energy-release rate. This occurs because the phase angle of the transverse shear components are in a sense that partially cancels the other components. It can be seen that for this geometry the drop in the energy-release rate associated with shear effects is fairly significant, even for relatively long spans and cracks ($a/h_1 > 10$). Furthermore, the phase angle tends to pure mode-II conditions in a fairly precipitous fashion at relative span lengths, L/h_1, significantly less than 10.

A final comment should be made about a three-point bend geometry in which there is an interfacial debond, but neither laminate is cracked. It can be shown that in the absence of a crack through one of the laminates, the effective bending moment, M, and axial load, N, acting on the interfacial crack are both equal to zero. Therefore, there is no driving force for delamination if the shear term is neglected. However, a small driving force can arise from the shear component in this configuration. For example, in the special case of a homogenous beam under three-point bending with a point load of F and with a delamination crack running along the central plane, the two shear loading terms are $V_d = F/4$ and $V_s = -F/2$. It can readily be shown that the energy-release rate for the delamination is pure mode-II and has a magnitude of

$$\frac{\bar{E} h \mathcal{G}}{F^2} = 0.0258. \tag{31}$$

This is small, but definitely non-zero.

5 Concluding remarks

In this paper, the procedures for developing analytical expressions for the energy-release rate and phase angle of beam-like geometries have been demonstrated for

three specific configurations: the edge-notch flexure geometry, the end-loaded split geometry, and the 3-point flexure geometry. Provided the basic loading parameters of axial load, moment, and transverse shear are known, general analytical solutions can be readily obtained by algebraic manipulation.

The energy-release rate associated with the moment and axial force components can be derived from steady-state energy balances, and are not affected by any considerations of the crack-tip field such as interfacial compliance, root rotation, elastic foundations, or cohesive zones [2, 13]. The effects of shear provide additional terms to these steady-state solutions. The shear component of the energy-release rate contains a contribution from the interaction of the shear force with the compliance associated with deformation at the crack tip [8]. The crack-tip deformation only affects the energy-release rate of beam-like geometries through this interaction with the shear component of the loading. Finally, it should be noted that additional corrections to the energy-release rate, beyond what is predicted from elasticity, can be provided by additional contributions to the crack-tip compliance such as the deformation of an adhesive layer. However, these corrections act only as corrections to the shear term. They do not provide corrections to the steady-state solutions associated with bending or axial loading [2, 13].

References

[1] Carlsson L A, Gillespie J W, and Pipes R B. On the analysis and design of the end-notched (ENF) specimen for mode II testing. *Journal of Composite Materials*, 20:594–604, 1986.

[2] Li S, Wang J, and Thouless M D. The effects of shear on delamination in layered materials. *Journal of the Mechanics and Physics of Fracture*, 52:193–214, 2004.

[3] Kanninen M F. An augmented double cantilever beam model for studying crack propagation and arrest. *International Journal of Fracture*, 9:83–91, 1973.

[4] Kanninen M F. A dynamic analysis of unstable crack propagation and arrest in the DCB test specimen. *International Journal of Fracture*, 10:415–430, 1974.

[5] Ding W and Kortschot M T. A simplified beam analysis of the end notched flexure mode II delmaination specimen. *Composite Structures*, 45:271–278, 1999.

[6] Corleto C R and Hogan H A. Energy release rates for the ENF specimen using a beam on an elastic foundation. *Journal of Composite Materials*, 29:1420–1436, 1995.

[7] He M-Y and Evans A G. Finite element analysis of beam specimens used to measure the delamination resistance of composites. *Journal of Composites Technology and Research*, 14:235–240, 1992.

[8] Andrews M G and Massabò R. The effects of shear and near tip deformations on energy release rate and mode mixity of edge-cracked orthotropic layers. *Engineering Fracture Mechanics*, 74:2700–2720, 2007.

[9] Wang Y and Williams J G. Corrections for mode II fracture toughness specimens of composite materials. *Composite Science and Technology*, 43:251–256, 1992.

[10] Suo Z and Hutchinson J W. Interface crack between two elastic layers. *International Journal of Fracture*, 43:1–18, 1990.

[11] Dundurs J. Edge-bonded dissimilar orthogonal elastic wedges. *Journal of Applied Mechanics*, 36:650–652, 1969.

[12] Leffler K, Alfredsson K S, and Stigh U. Shear behaviour of adhesive layers. *International Journal of Solids and Structures*, 44:530545, 2007.

[13] Parmigiani J P and Thouless M D. The effects of cohesive strength and toughness on mixed-mode delamination of beam-like geometries. *Engineering Fracture Mechanics*, 74:2675–2699, 2007.

6 Appendix

6.1 Table of phase angles ($\beta = 0$) [2]

H	α	**-0.8**	**-0.6**	**-0.4**	**-0.2**	**0.0**	**0.2**	**0.4**	**0.6**	**0.8**
0.0	ψ_M	-43.3°	-42.3°	-41.0°	-39.6°	-37.9°	-35.9°	-33.4°	-30.1°	-24.9°
	ψ_{V_d}	+5.0°	+4.0°	+3.0°	+2.0°	+0.7°	-0.5°	-1.7°	-3.1°	-4.8°
	ψ_{V_s}	+5.0°	+4.0°	+3.0°	+2.0°	+0.7°	-0.5°	-1.7°	-3.1°	-4.8°
0.2	ψ_M	-43.0°	-41.3°	-39.4°	-37.3°	-34.8°	-31.8°	-28.1°	-22.9°	-14.3°
	ψ_{V_d}	+4.6°	+3.4°	+2.1°	+0.7°	-0.6°	-2.1°	-3.6°	-5.1°	-6.6°
	ψ_{V_s}	+4.3°	+2.6°	+0.8°	-1.2°	-3.5°	-6.0°	-8.7°	-11.7°	-15.1°
0.4	ψ_M	-41.5°	-38.4°	-35.1°	-31.6°	-27.5°	-22.8°	-16.9°	-8.9°	+4.0°
	ψ_{V_d}	+4.5°	+3.3°	+1.9°	+0.6°	-0.8°	-2.1°	-3.5°	-4.8°	-5.9°
	ψ_{V_s}	+3.2°	+0.6°	-2.0°	-4.6°	-7.4°	-10.0°	-12.6°	-15.2°	-17.9°
0.6	ψ_M	-39.2°	-34.1°	-29.1°	-23.8°	-18.1°	-11.8°	-4.3°	+5.2°	+18.5°
	ψ_{V_d}	+4.5°	+3.3°	+2.1°	+0.8°	-0.5°	-1.8°	–3.1°	-4.3°	-5.3°
	ψ_{V_s}	+1.6°	-1.9°	-4.9°	-7.6°	-10.5°	-12.8°	-15.0°	-17.1°	-19.1°
0.8	ψ_M	-36.0°	-28.8°	-22.1°	-15.4°	-8.6°	-1.3°	+6.6°	+15.8°	+27.3°
	ψ_{V_d}	+4.7°	+3.5°	+2.3°	+1.0°	-0.3°	-1.5°	-2.7°	-3.9°	-5.0°
	ψ_{V_s}	-0.5°	-4.6°	-7.7°	-10.2°	-13.0°	-14.9°	-16.7°	-18.3°	-19.8°
1.0	ψ_M	-32.4°	-23.0°	-14.9°	-7.3°	-0.0°	+7.3°	+14.9°	+23.0°	+32.4°
	ψ_{V_d}	+4.8°	+3.7°	+2.5°	+1.3°	0.0°	-1.3°	-2.4°	-3.6°	-4.9°
	ψ_{V_s}	-3.0°	-7.5°	-10.5°	-12.7°	-15.1°	-16.3°	-17.7°	-19.0°	-20.2°

6.2 Table of numerical constants ($\beta = 0$) for the shear components of the energy-release rate [2]

H	α	**-0.8**	**-0.6**	**-0.4**	**-0.2**	**0.0**	**0.2**	**0.4**	**0.6**	**0.8**
0.0	f_{V_d}	1.64	1.69	1.76	1.84	1.94	2.09	2.29	2.61	3.28
	f_{V_s}	1.64	1.69	1.76	1.84	1.94	2.09	2.29	2.61	3.28
0.2	f_{V_d}	1.635	1.687	1.753	1.833	1.940	2.089	2.300	2.654	3.412
	f_{V_s}	1.607	1.628	1.662	1.715	1.791	1.902	2.075	2.380	3.055
0.4	f_{V_d}	1.645	1.708	1.784	1.881	2.009	2.186	2.439	2.865	3.800
	f_{V_s}	1.531	1.507	1.510	1.545	1.618	1.729	1.908	2.214	2.851
0.6	f_{V_d}	1.663	1.739	1.836	1.954	2.106	2.314	2.619	3.125	4.250
	f_{V_s}	1.413	1.354	1.351	1.386	1.458	1.573	1.746	2.023	2.518
0.8	f_{V_d}	1.684	1.781	1.898	2.037	2.217	2.460	2.809	3.394	4.704
	f_{V_s}	1.282	1.206	1.206	1.247	1.323	1.434	1.590	1.812	2.137
1.0	f_{V_d}	1.711	1.829	1.968	2.127	2.335	2.605	3.003	3.665	5.127
	f_{V_s}	1.150	1.077	1.088	1.133	1.207	1.306	1.438	1.607	1.787

Figure Captions

Figure 1: The geometry of **(a)** an edge-notched flexure specimen, **(b)** an end-loaded split specimen (ELS) and **(c)** a 3-point bend specimen. Each geometry consists of two unequal laminates of thicknesses h_1 and h_2 and moduli $\bar{E}_1$ and $\bar{E}_2$ bonded together with a crack of length a along the interface.

Figure 2: The bending moments, axial loads and transverse shear loads acting on each segment of a cracked beam-like geometry.

Figure 3: The fundamental problems for delamination of beam-like geometries: **(a)** axial load, **(b)** moment, **(c)** double transverse shear force, **(d)** single transverse shear load.

Figure 4: The effects of crack length and thickness ratio on **(a)** the energy-release rate and **(b)** the phase angle of an ENF beam, with no modulus mismatch.

Figure 5: The effects of crack length and modulus mismatch on **(a)** the energy-release rate and **(b)** the phase angle of an ENF beam, with $h_1 = h_2 = h$. Negative values of the modulus mismatch parameter α simply change the sign of the phase angle.

Figure 6: The effects of crack length and thickness ratio on **(a)** the energy-release rate and **(b)** the phase angle of an ELS configuration with no modulus mismatch.

Figure 7: The effects of crack length and modulus mismatch on **(a)** the energy-release rate and **(b)** the phase angle of an ELS configuration with $h_1 = h_2 = h$.

Figure 8: The effects of span length and modulus ratio on **(a)** the energy-release rate and **(b)** the phase angle of a 3-point bend geometry, with laminates of equal thickness. A comparison to the steady-state solutions, calculated ignoring shear, can be seen from the dashed lines at very large span lengths.

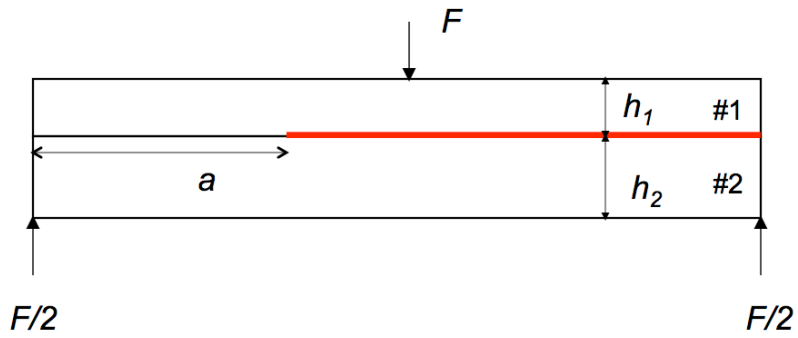

a)

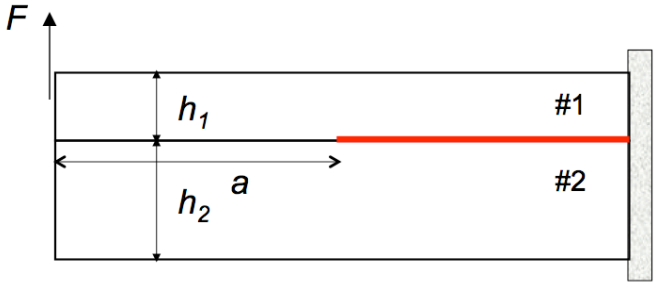

b)

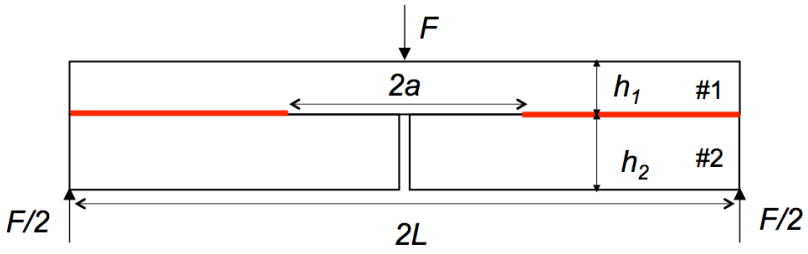

c)

Figure 1

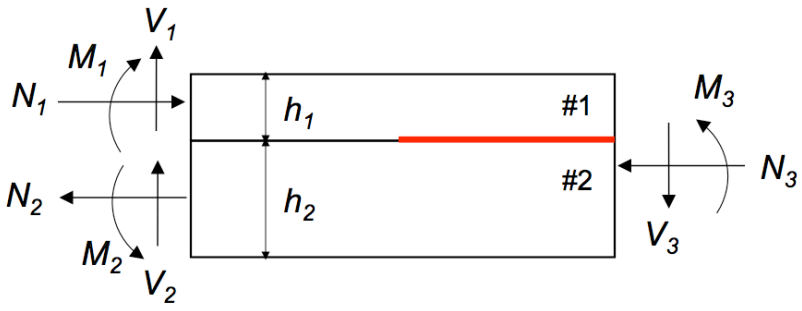

Figure 2

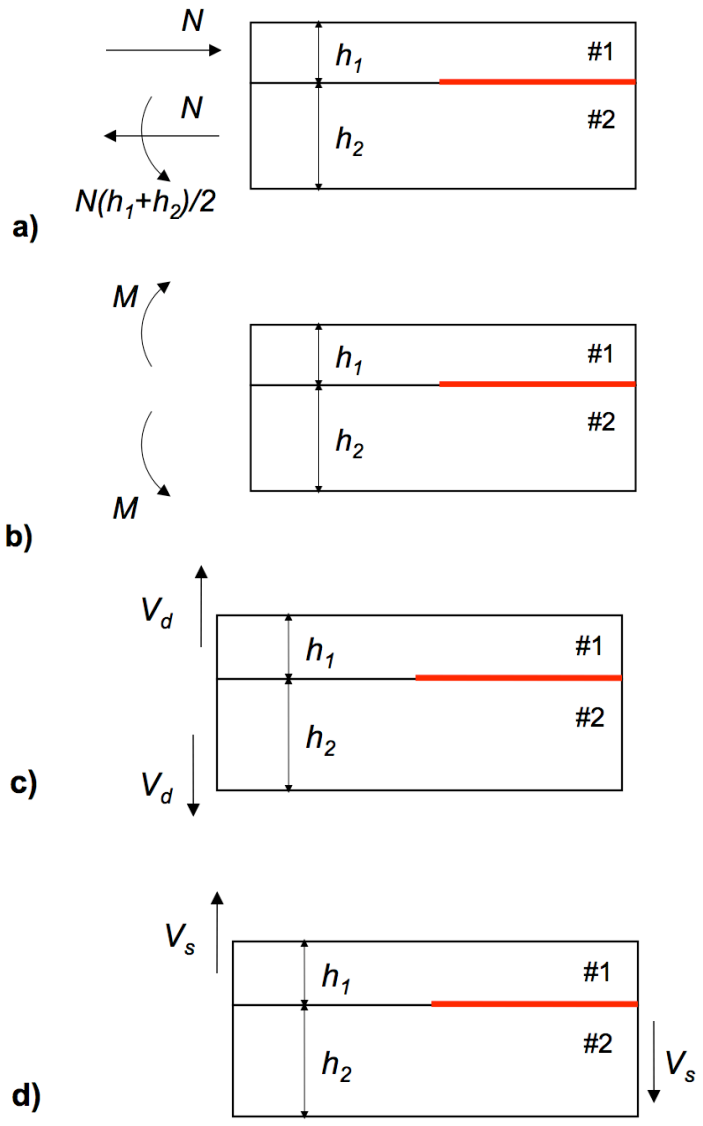

Figure 3

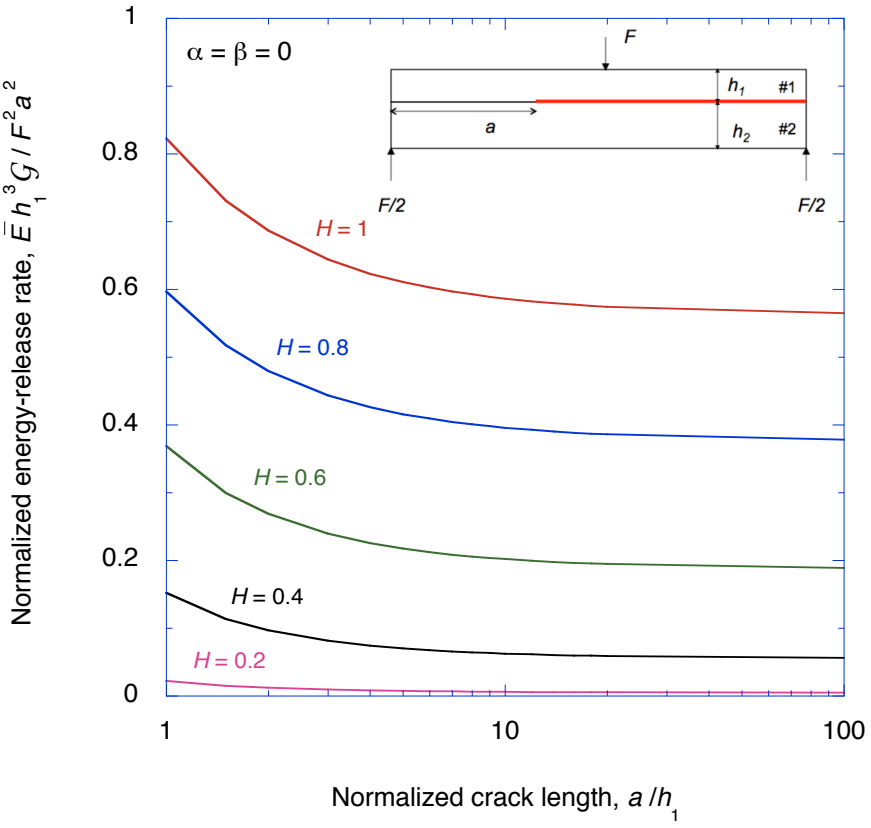
α = β = 0
F
h1
#1
h2
#2
a
F/2
F/2
H = 1
H = 0.8
H = 0.6
H = 0.4
H = 0.2
Normalized energy-release rate, $\bar{E} h_1^3 \mathcal{G} / F^2 a^2$
Normalized crack length, a / h_1
0
0.2
0.4
0.6
0.8
1
1
10
100

Figure 4a

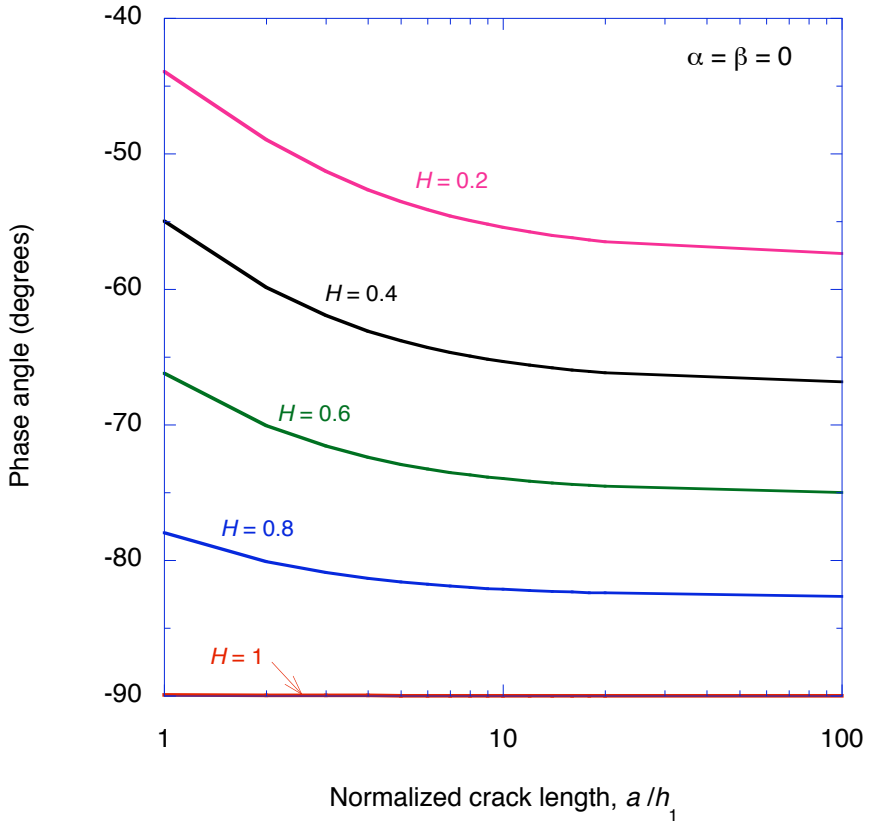
-40
-50
-60
-70
-80
-90
Phase angle (degrees)
α = β = 0
H = 0.2
H = 0.4
H = 0.6
H = 0.8
H = 1
1
10
100
Normalized crack length, a /h1

Figure 4b

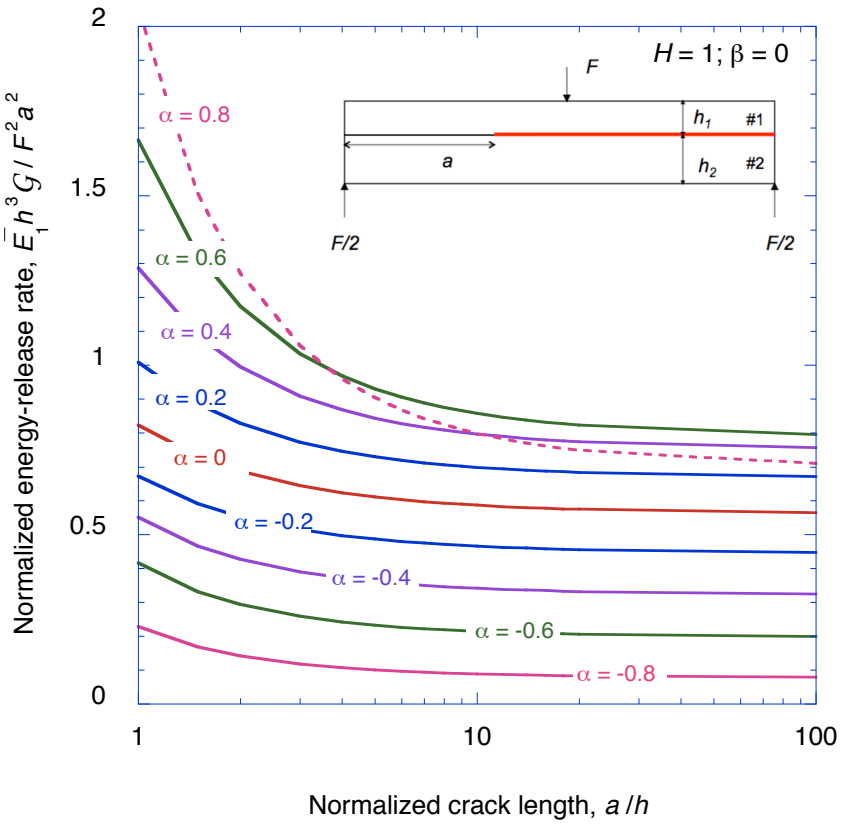
Normalized energy-release rate, $\bar{E}_1 h^3 \mathcal{G} / F^2 a^2$
Normalized crack length, a/h
$H = 1; \beta = 0$
F
F/2
F/2
a
h_1
#1
h_2
#2
α = 0.8
α = 0.6
α = 0.4
α = 0.2
α = 0
α = -0.2
α = -0.4
α = -0.6
α = -0.8
2
1.5
1
0.5
0
1
10
100

Figure 5a

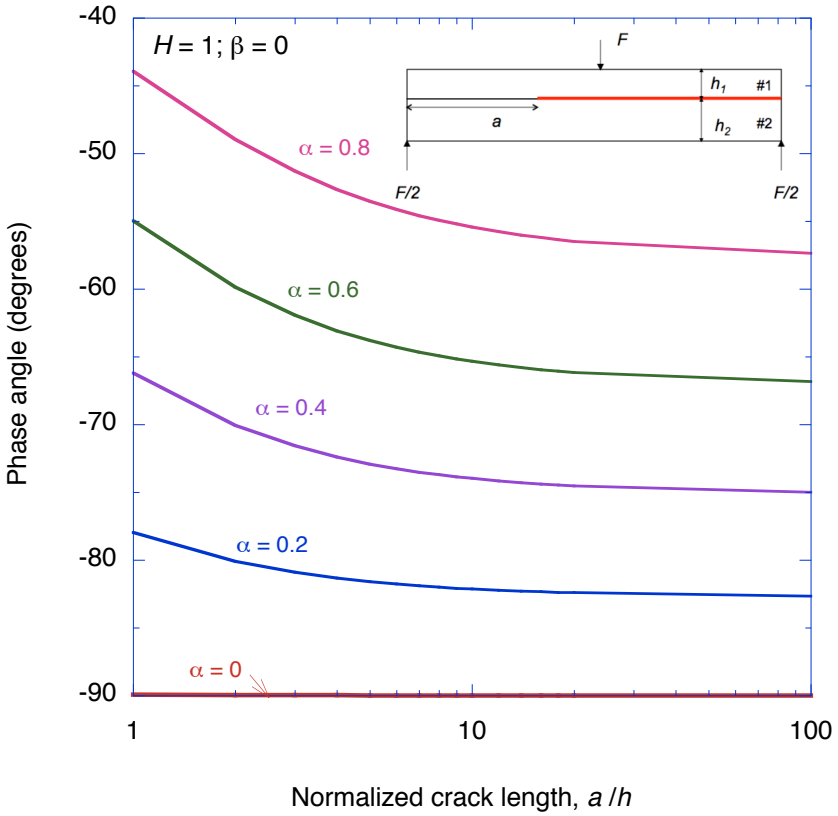
H = 1; β = 0
F
h1
#1
h2
#2
a
F/2
F/2
α = 0.8
α = 0.6
α = 0.4
α = 0.2
α = 0
-40
-50
-60
-70
-80
-90
1
10
100
Phase angle (degrees)
Normalized crack length, a /h

Figure 5b

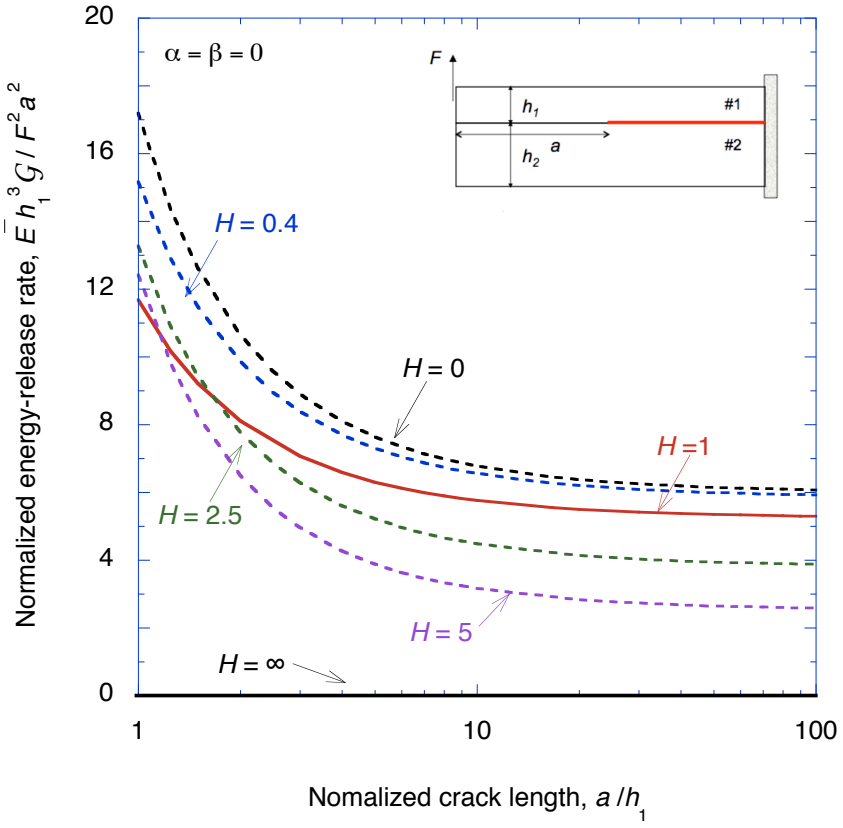
20
16
12
8
4
0
1
10
100
α = β = 0
F
h1
#1
h2
a
#2
H = 0.4
H = 0
H =1
H = 2.5
H = 5
H = ∞
Normalized energy-release rate, $\bar{E} h_1^3 \mathcal{G} / F^2 a^2$
Nomalized crack length, a / h_1

Figure 6a

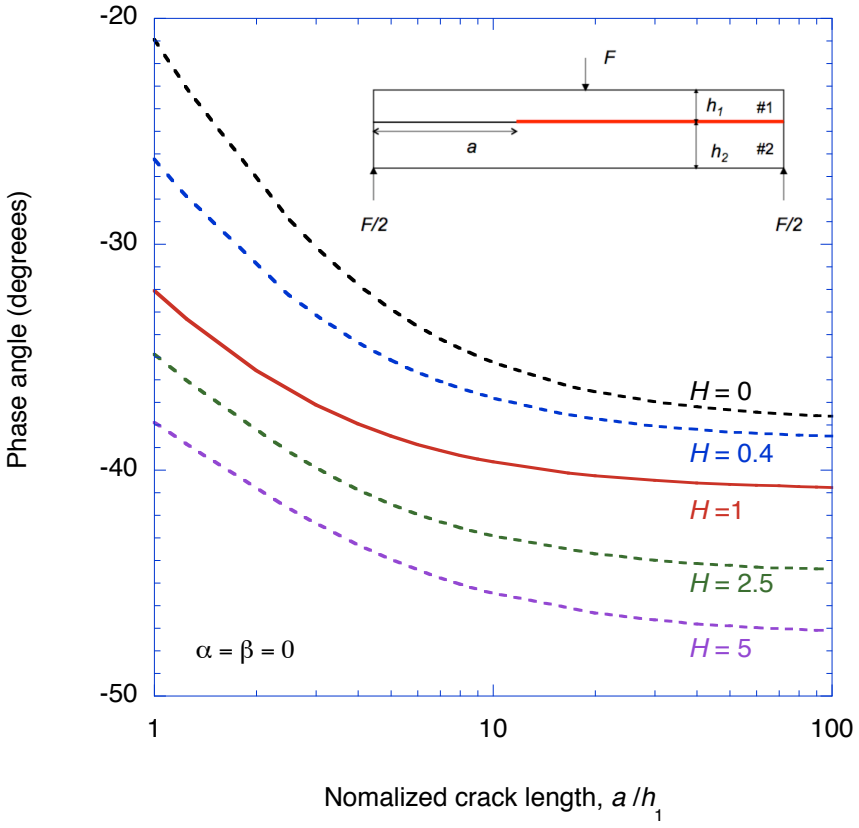
-20
-30
-40
-50
1
10
100
Phase angle (degrees)
Nomalized crack length, a /h1
F
h1
#1
a
h2
#2
F/2
F/2
H = 0
H = 0.4
H =1
H = 2.5
H = 5
α = β = 0

Figure 6b

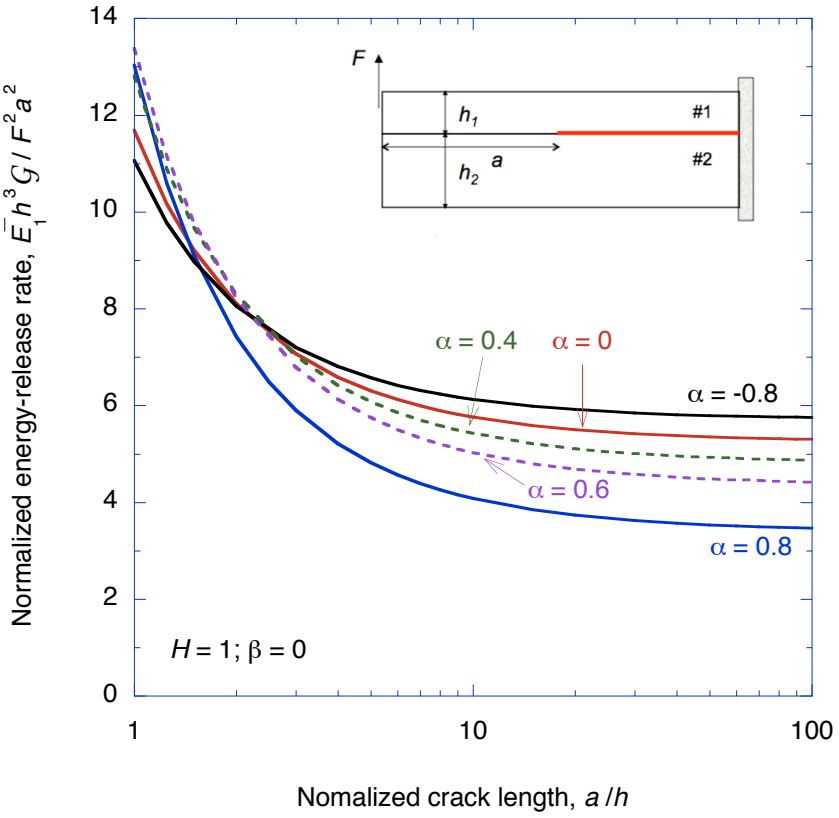
Normalized energy-release rate, $\bar{E}_1 h^3 \mathcal{G} / F^2 a^2$
Nomalized crack length, a/h
F
h_1
h_2
a
#1
#2
α = 0.4
α = 0
α = -0.8
α = 0.6
α = 0.8
H = 1; β = 0
0
2
4
6
8
10
12
14
1
10
100

Figure 7a

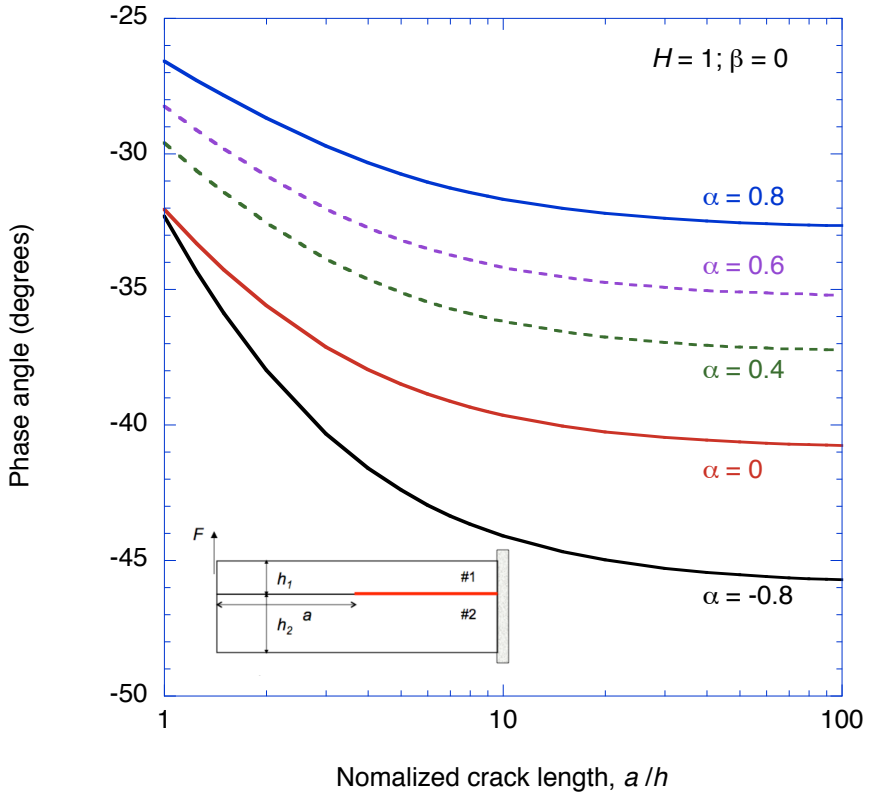
-25
-30
-35
-40
-45
-50
1
10
100
Phase angle (degrees)
Nomalized crack length, a /h
H = 1; β = 0
α = 0.8
α = 0.6
α = 0.4
α = 0
α = -0.8
F
h1
h2
a
#1
#2

Figure 7b

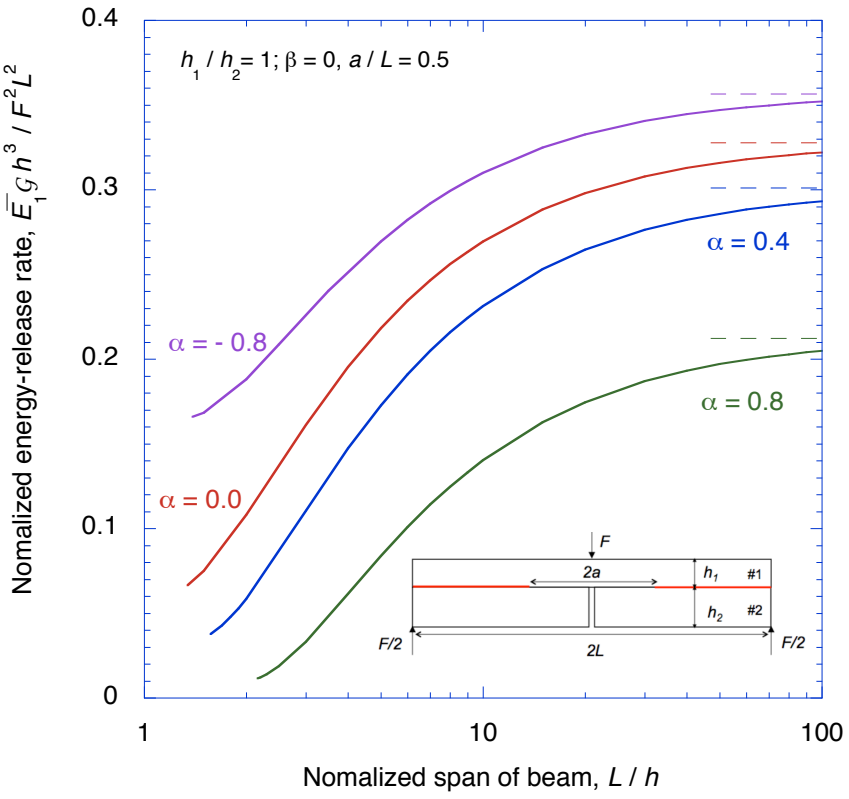
$h_1 / h_2 = 1$; $\beta = 0$, $a / L = 0.5$
α = - 0.8
α = 0.0
α = 0.4
α = 0.8
F
2a
h_1 #1
h_2 #2
F/2
2L
F/2
0.4
0.3
0.2
0.1
0
1
10
100
Nomalized energy-release rate, $\bar{E}_1 \mathcal{G} h^3 / F^2 L^2$
Nomalized span of beam, L / h

Figure 8a

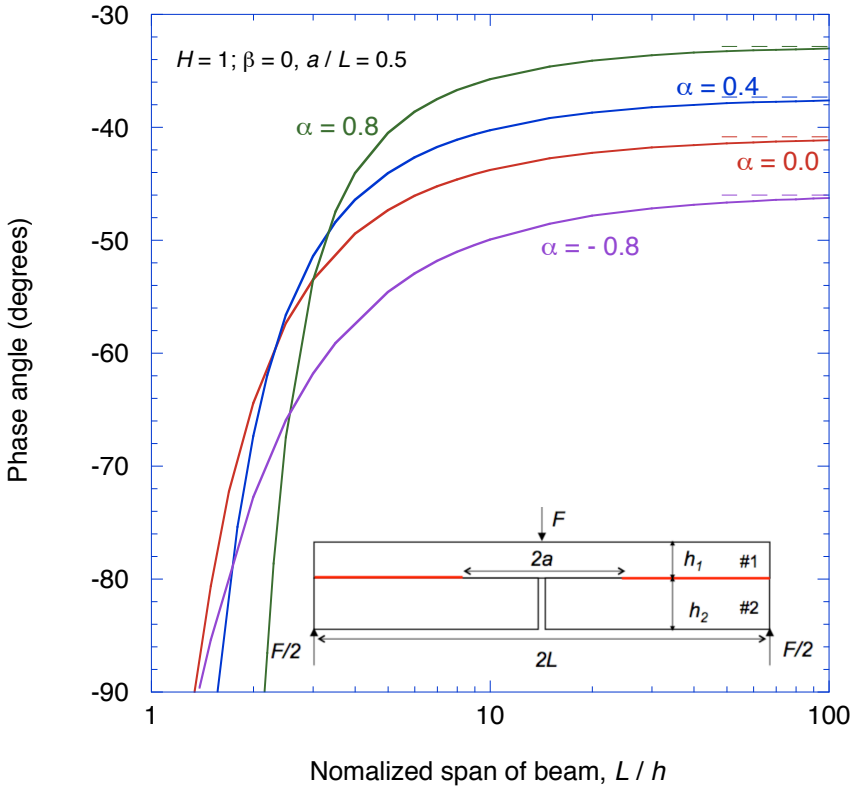
H = 1; β = 0, a / L = 0.5
α = 0.4
α = 0.8
α = 0.0
α = - 0.8
-30
-40
-50
-60
-70
-80
-90
1
10
100
Phase angle (degrees)
Nomalized span of beam, L / h
F
2a
h1
#1
h2
#2
F/2
2L
F/2

Figure 8b